

Field Test of Detection and Characterization of Subsurface Ice Using Broadband Spectral Induced Polarization

Robert E. Grimm

David E. Stillman

Planetary Science Directorate

Southwest Research Institute

1050 Walnut St. #300

Boulder, Colorado 80302

USA

Submitted to

Permafrost and Periglacial Processes

as a

Short Communication

March 11, 2014

Keywords: spectral induced polarization, electrical properties, frozen soil.

Abstract

Low-frequency (LF, $\ll 100$ Hz) electrical conductivity is useful in identifying unfrozen ground in periglacial environments, but cannot distinguish whether frozen materials are dry or ice-rich. The electrical polarization of ice is a unique signature that is manifested as an increase in conductivity at high frequencies (HF, $\gg 100$ Hz). From laboratory measurements of samples collected at the US Army Permafrost Tunnel (Fox, Alaska), we find temperature-dependent relationships between ice volume fraction and chargeability (defined as the HF-normalized difference in HF and LF conductivities). We report the first field detection of the polarization of ice, using a broadband spectral induced polarization (SIP) system at the Permafrost Tunnel. Variations in ice content determined from SIP correlated with geology, in particular, the inferred position of an ice wedge within the tunnel wall. By comparing ensemble laboratory and field spectra, we found a best-fitting ice temperature of $-3 \pm 1^\circ\text{C}$. This in turn calibrates the ice content and yielded 50-100% ice in the tunnel walls, in good agreement with sampling. Temperature uncertainties can be reduced by fitting the specific dielectric relaxation frequency and not just the envelope of spectra. Broadband SIP is a promising tool for field measurement of subsurface ice content and temperature.

1. Introduction

Measurement of the ice content in permafrost is important to understanding evolution of periglacial landforms (e.g., French, 2007), the ecology of permafrost regions (Jorgenson and Osterkamp, 2005), the impact of permafrost melting on the global carbon inventory (Schuur *et al.*, 2008), and the risk to infrastructure due to frost heave and melting (e.g., Heginbottom *et al.*, 2012). Classical indicators of air temperature, surficial geology, and aerial or satellite mapping give only large-scale classification, whereas coring and excavation are tedious and highly localized. Geophysical methods have the potential to fill a critical gap between aerial imaging and core sampling (see reviews by Scott *et al.*, 1990, Kneisel *et al.*, 2008, and Hauck, 2013). Their main strength has been to identify frozen vs. unfrozen ground, e.g., delineating the active layer and the base of permafrost. Electrical and electromagnetic methods have been widely applied because the quasi-static (“DC”) conductivity of ice σ_s is very low compared to soils containing unfrozen water. Unfortunately, both dry materials and totally frozen ice-rich materials have low DC conductivity (e.g., Minsley *et al.*, 2011), so there is substantial ambiguity about ice content. A recent approach to joint inversion of seismic and electrical data for rock, ice, water, and air content (Hauck *et al.*, 2011) is useful for the near-uniform porosity and low clay content of rock glaciers, but is inappropriate for most permafrost soils.

There is, however, a unique property of ice that heretofore has not been exploited in the field: its electrical polarization. Whereas conductivity or resistivity measures energy dissipation through charge motion, electrical susceptibility or permittivity measures energy storage through separation of bound charges. Ice polarization in natural and synthetic permafrost samples has been characterized in the laboratory (Olhoeft, 1977; Bitelli *et al.*, 2004; Stillman *et al.*, 2010) and there is an even longer history of lab measurements of ice with soluble impurities (see Petrenko

and Whitworth, 1999, for a review and Grimm *et al.*, 2008 and Stillman *et al.*, 2013, for newer findings). Yet the geophysical approach known as “induced polarization” has lagged the laboratory for permafrost, lacking any mention in recent reviews (Kneisel *et al.*, 2008; Hauck, 2013). The development of broadband, high-impedance field systems now enables geophysical measurements for ice content. In this paper, we first review the electrical properties of permafrost. We show how the classical frequency-domain chargeability is directly related to ice content as measured from laboratory data. We apply this technique to pilot field measurements in permafrost. Finally, we describe temperature corrections to the data and suggest protocols for future surveys and for long-term monitoring.

2. Background and Laboratory Characterization

Materials respond to time-varying electric fields by a combination of dissipation and storage of energy and so can be represented by a single, frequency-dependent, complex number. Here we focus on complex conductivity $\sigma^* = \sigma' + i\sigma''$ for the theory but we also use real resistivity $\rho' = \sigma' / |\sigma^*|^2$ and phase $\phi = \tan^{-1}(\sigma''/\sigma')$ for data as this is a common format in geophysics. The real conductivity σ' (or ρ') controls energy dissipation and the imaginary conductivity σ'' determines the energy storage.

The polarizability or energy storage in ice is due to protonic point defects: lattice sites where hydrogen atoms are improperly configured with respect to adjacent H₂O molecules (e.g., Petrenko and Whitworth, 1999). These charge defects (specifically, Bjerrum L-defects) can be rotated and follow a frequency dependent behavior called a dielectric relaxation. At low frequency, bound charges can be fully separated over one cycle, manifesting the full polarization. At high frequency, the relevant charges cannot keep up with the applied field and

are essentially unpolarizable. At some intermediate frequency—the relaxation frequency—charges move over nearly their full allowed extent over the course of the applied cycle.

One useful description of a dielectric relaxation is the Cole-Cole formula (Cole and Cole, 1941)

$$\sigma^* = \sigma_s + \frac{\sigma_s m (i\omega\tau)^{1-\alpha}}{1 + (1-m)(i\omega\tau)^{1-\alpha}} + i\omega\epsilon_0\epsilon_\infty \quad (1)$$

where σ_s is the static or “DC” conductivity, m is the chargeability, ω is the angular frequency, τ is the relaxation time constant, α is the distribution parameter, ϵ_0 is the permittivity of free space, and ϵ_∞ is the permittivity at infinite frequency. This equation represents three circuit elements in parallel: from left to right, a resistor that controls low frequencies, a frequency-dependent impedance controlling the relaxation, and a capacitor that controls high frequencies. In real materials, multiple polarization mechanisms can exist, so the second term is repeated with distinct properties for each relaxation. The last term is commonly omitted in geophysics where maximum frequencies are small compared to those studied here, but it is essential to measuring time constants correctly and for agreement with other fields such as material science (see Olhoeft, 1985, and Jones, 1997). The chargeability is the fractional change in conductivity across the dielectric relaxation

$$m = \frac{\sigma'_\infty - \sigma'_s}{\sigma'_\infty} = \frac{\rho'_s - \rho'_\infty}{\rho'_s} \quad (2)$$

where σ'_∞ (ρ'_∞) is the real conductivity (resistivity) at infinite frequency. The phase ϕ gives the lag between current injected into a sample and the voltage measured across it. Ohmic dissipation is maximized at the relaxation frequency, but ϕ is smallest a factor of 2π higher in frequency.

Note that $\alpha = 0$ for the classic Debye relaxation.

For “pure” ice, in which all protonic point defects are intrinsic, the dielectric is close to Debye form and the relaxation frequency increases from 4 to 11 kHz as temperature is increased from -10°C to 0°C . The corresponding minimum phase lag moves from 13 to 35 kHz. With the phase conventionally plotted as negative (lag), the minimum phase lag looks like a peak (**Fig. 1**) and we sometimes refer to it as such by analogy with spectra in other disciplines.

We measured the frequency- and temperature-dependent complex conductivity of samples of the Fairbanks silt acquired from within the US Army Cold Regions Research and Engineering Laboratory (CRREL) Permafrost Tunnel near Fox, Alaska (Sellman, 1967; 1972). We selected this location for an initial attempt at in situ ice detection and characterization using broadband complex conductivity because the site was well-characterized in the literature (e.g., Arcone, 1984; Bjella et al., 2008) and by previous DC-resistivity surveys (Dinwiddie *et al.*, 2009). Furthermore, the ice content in and around the tunnel was known to be very high. Laboratory procedures are described by Grimm *et al.* (2008) and Stillman *et al.* (2010). The measurement bandwidth was 1 mHz – 1 MHz. Samples were measured with ice intact and then dried and rehydrated with different water contents.

The complex conductivity spectra (Fig. 1) are dominated by σ_s at low frequency and the ice and relaxation at high frequency. Note that, in contrast to typical induced-polarization studies at temperatures above freezing, phases in frozen materials can be very large (tens of degrees negative) because low σ_s transitions the response from resistive to capacitive around 100 Hz. The ice relaxation is evident only because σ_s is low and does not “short-circuit” the entire spectrum.

Soils with a high specific surface area (e.g., clay) can seriously complicate the spectra

(Olhoeft, 1976; Bitelli *et al.*, 2004; Stillman *et al.*, 2010) due to the increased amounts of adsorbed water and formation of ice with more defects near the pore walls. These effects are evident in Fairbanks silt (~25v% montmorillonite or clay), but can be accounted for by fitting additional relaxations to the permafrost conductivity spectra (Stillman *et al.*, 2010).

The ice relaxation frequencies in the Fairbanks silt are close to that of pure H₂O (**Fig. 2**). This is consistent with ice formation by slow freezing from a liquid, in which soluble impurities are efficiently excluded (Grimm *et al.*, 2008). Chloride, the principal ice-soluble impurity, substitutes for oxygen but engenders extrinsic protonic defects due to its different charge. In contrast, polar meteoric ice, which nucleates in the atmosphere, incorporates up to 50% of the soluble impurities in the lattice (Stillman *et al.*, 2013): this causes much faster dielectric relaxation.

Given the richness of the laboratory complex-conductivity spectra, a commensurate inversion from field data is desirable. However, this objective has not been fully realized: Kemna *et al.* (2000) inverted laboratory scale model data for the 3D distribution of a single relaxation, but there have been no subsequent full-scale field analyses. We attribute this to the lower data density and signal-to-noise ratio (including the effects of correlated noise like inductive coupling) of contemporary field experiments. Furthermore, inversions must in practice be able to fit multiple relaxations in order to isolate a single mechanism of interest.

We therefore sought a simple parameterization of the spectrum that captured the essential ice signature and would be suitable for field data. The normalized difference in real conductivity measured between “high” and “low” frequencies approximates the chargeability of the dielectric relaxation. From the parameters of the field system and the results of our initial test (see below), we selected the conductivities at 10 Hz and 20 kHz as representative of the static- and infinite-

frequency endmembers, so

$$m \approx \frac{\rho'_{10Hz} - \rho'_{20kHz}}{\rho'_{10Hz}} \quad (3)$$

The chargeability has the convenient range [0,1].

At a fixed temperature, the chargeability of the Fairbanks silt (**Fig. 3**) varies monotonically with ice volume fraction θ (apart from small experimental errors). We fit simple a polynomial to the laboratory data of $\theta(m)$ at each measurement temperature. Note, however, that a 1°C difference in temperature translates to 10–20% uncertainty in ice content. This will be seen to influence the accuracy of ice-volume estimation. Furthermore, this single broadband parameter will include any polarizability due to adsorbed water in addition to the ice signature.

3. Field Methods

In the field, broadband frequency domain complex-conductivity measurements are known as Spectral Induced Polarization (SIP). SIP field surveys are geometrically identical to classical DC Resistivity. The measured voltage and its phase between any pair of transmit and receive dipoles yields a spectrum of apparent resistivity and phase as functions of electrode position and offset, which are then inverted to recover true resistivity and phase as functions of surface position and depth.

We used the SIP Fuchs III by Radić Engineering of Berlin, Germany. This system has 20-kHz bandwidth, high input impedance (10 GΩ), sends signals to the transmitter dipole and from multiple receiver dipoles by fiber-optic cable, and incorporates a remote-reference dipole for noise reduction. The Fuchs enables field measurements in cold regions because (1) the high input impedance allows signals to be measured in spite of high contact resistance with frozen ground, (2) the large bandwidth is sensitive to enough of the increase in conductivity in

frequency and change in phase to characterize the strength of the ice dielectric relaxation, and hence ice content, and (3) resistive ground and optical isolation allow electrode spreads of tens of meters long without inductive coupling, even at high frequency. This in turn means investigation depths of order 10s of m can be achieved.

We tested several approaches to inversion, all using RES2DINV (Loke and Barker, 1996; Geotomo Software: www.geotomosoft.com). In the first, the real part of the resistivity at 10 Hz and 20 kHz were separately inverted and compared to form a chargeability image. This does not exploit the physical link between frequencies and so as expected produced excessive random or systematic errors. We did not find the IP procedures in RES2DINV, which use DC resistivity and chargeability, to be effective either, perhaps partly due to the limited density of our dataset.

We discovered a third approach that was successful: by using the time-lapse feature of RES2DINV, we inverted the entire spectrum of 24 real resistivities between 10 Hz and 20 kHz and derived chargeability from the result. The time-lapse algorithm assumes that each measurement is derived from the previous one and so applies a regularization across successive measurements (Kim, 2009). By treating the lowest frequency as “zero time” and each successive frequency in the spectrum as a “time step,” smooth inversions could be obtained. We assigned equal weight to reducing the differences between the models (images) at different frequencies and reducing the individual model roughness. This technique is therefore a compromise between inverting individual frequencies and direct inversion for Cole-Cole parameters. Also note that we did not fit phase explicitly, but this can be checked a posteriori using the Kramers-Kronig relations.

The Permafrost Tunnel comprises a horizontal adit and a smaller winze that slopes downward and away from the adit (**Fig. 4**). Here we report an SIP survey performed on the adit

side of the winze, on a line positioned from 1 to 17 m from the adit-winze intersection. The electrodes were emplaced into the winze wall and so the plane of the 2D survey is horizontal, in the plane of Fig. 4. The survey used dipole lengths a of 1 and 2 m and offsets $n = 1-6$ as space allowed. We also did a cross-tunnel test and a survey on the surface above the tunnel: although the apparent resistivity spectra confirm those of the principal survey, fewer measurements and lower SNR did not produce satisfactory inversions.

We surveyed in both forward and reciprocal configurations. Reciprocals of the winze survey were typically in good agreement. However, many spectra had positive phase and so were discarded. We attribute much of this effect to abundant metal artifacts in the tunnel. This left 40 independent measurements (spectra) for inversion.

4. Results and Discussion

Figure 5 shows the results of the Permafrost Tunnel SIP survey, including the resistivity images at 10 Hz and 20 kHz, the chargeability derived from their normalized difference, and the ice content inferred from laboratory relationships. As required, $\rho'_{10\text{Hz}} \geq \rho'_{20\text{kHz}}$ everywhere, so that $m \geq 0$ always. The chargeabilities are high, often approaching the maximum value of unity. The main feature of Fig. 5 is a zone of very high ice content that slants from the surface through the full 2-m maximum depth of the image. This correlates very well with the position of an ice wedge, whose trace is inferred from exposures in both the winze and adit (Arcone, 1984). A zone of low ice content appears just before the ice wedge; this correlates with a region of prominent laminations and organic inclusions in the Fairbanks silt (Kanevskiy, 2008).

The mean ice content in Fig. 6c is 80% and the standard deviation is 11%. We determined the ice content of seven samples in the winze (distributed over both walls and the ceiling) to be

76 ± 18%. This agreement is very good overall: equality of the medians can only be rejected at $p = 0.49$ using the Wilcoxon rank-sum test (with the image downsampled to the number of original data). However, the samples were not necessarily random, being chosen for variety. Furthermore, point-by-point comparisons are mediocre, because of the extreme heterogeneity in permafrost stratigraphy and structure (see map of winze wall by Kanevskiy, 2008). Sellman (1967) reported ice content in 45 samples from the adit, including 4 locations with multiple (5–9) closely spaced samples. Variations up to 20% exist within these dense sampling locales, with standard deviations of 3–6%. After averaging these locales, the reweighted ice content for Sellman’s adit samples is 67% ± 7%. Variability within sampling locales can therefore be comparable to that between locales. Also note that, after eliminating two of our samples taken from ice wedges (which Sellman avoided), ice contents of our winze samples are consistent with the same population as Sellman’s adit samples (Wilcoxon rank-sum $p = 0.43$).

The mapping to ice content is shown at a constant temperature of -3°C . This was determined by visually comparing the distribution of all inverted spectra in the image to the laboratory spectra (**Fig. 6**). The accuracy for this simple approach is $\pm 0.5\text{--}1^{\circ}\text{C}$. This can be improved not only by formal chi-squared procedures, but by directly fitting the relaxation frequency. Fitting errors for this procedure on laboratory data are $\pm 0.5^{\circ}\text{C}$ at -3°C and below (premelting flattens the curves at higher temperatures and relaxation frequencies are indistinguishable), and suitable long-term integration could yield accuracies $\pm 0.1^{\circ}\text{C}$.

The mean ground temperature of -3°C inferred here is higher than that measured three decades ago in wall cores (-4.6 to -7°C ; Arcone, 1984). More recently, air temperatures in the tunnel were between -3 and -2°C , although there is evidence for excursions close to or exceeding 0°C at the rear of the adit (Bjella *et al.*, 2008).

5. Conclusion

We measured the complex conductivity of natural and reconstituted permafrost samples in the laboratory from 1 mHz – 1 MHz. We found that the spectra were dominated by DC conductivity and the dielectric relaxation of ice. The classical frequency-domain definition of chargeability increases monotonically with ice content but is temperature-dependent. We performed dipole-dipole spectral induced polarization (SIP) field surveys over the bandwidth 10 Hz – 20 kHz and found that the field spectra were similar to lab measurements. The mean fractional ice volume derived from the field data using laboratory chargeability relations agreed well with the mean measured from samples, but point comparisons were ineffective due to local sampling heterogeneity in the tunnel up to 20%. The zone of highest ice content correlated well with a known ice wedge and the zone of lowest ice content was associated with prominent laminations and organic inclusions in the host silt.

An important part of the workflow is determining the ground temperature from the spectra, as this is required for selection of the correct curve relating chargeability to ice content. Visual inspection constrains the temperature to better than 1°C and formal procedures achieve 0.5°C or better. We envision that higher SNR from both spatially denser setups and longer integration times will reduce temperature errors to the vicinity of 0.1°C. With such accuracy, spatial variations in temperature can be mapped without drilling, e.g., geothermal gradients or top-down propagation of long-term surface-temperature variations.

Outstanding issues focus on productivity and generalizability. Can procedures be developed that achieve high data density but move more quickly than the standard SIP setup? Does each site require a full suite of laboratory measurements for calibration of the chargeability? We

chose the Fox Permafrost Tunnel for initial tests because of known high ice content and prior geophysical characterization, but a site incorporating a full range from zero to near 100% ice would provide robust validation. The techniques demonstrated here will have value for permafrost studies, infrastructure assessment, and perhaps extraterrestrial exploration (Grimm and Stillman, 2011).

6. Acknowledgements

We thank Kevin Bjella and Margaret Cysewski (US Army Cold Regions Research and Engineering Laboratory) for support at the Fox Permafrost Tunnel, and Ronald McGinnis and Cynthia Dinwiddie (SwRI) for discussion of prior geophysical surveys there. This work was funded by SwRI Internal Research Grants R8374 and R8422.

7. References

- Arcone, SA. 1984. Pulse transmission through frozen silt. *CRREL TR-84-17*, 19 pp.
- Bitelli 04
- Bjella, K, Tantillo T, Weale J, Lever J. 2008. Evaluation of the CRREL Permafrost Tunnel. *ERDC/CRREL TR-08-11*, 66 pp.
- Cole KS, Cole RH. 1941. Dispersion and adsorption in Dielectrics I: Alternating current characteristics. *J. Chem. Phys.* **9**: 341-352.
- Dinwiddie CL, McGinnis RN, Stillman DE, Grimm RE, Hooper DM, Bjella K. 2009. Integrated Geophysical Examination of the CRREL Permafrost Tunnel's Fairbanks Silt Units, Fox, Alaska. *Eos Trans. AGU*, **90(52)**, Fall Meet. Suppl., Abstract C41A-0429.
- French HM. 2007. *The Periglacial Environment*, 3rd ed. Wiley.
- Grimm RE, Stillman DE. 2011. Progress in prospecting for near-surface H₂O on the Moon and Mars with dielectric spectroscopy. *Lunar Planet. Sci. Conf XII*, Lunar Planet. Institute,

Houston, #2550.

- Grimm RE, Stillman DE, Dec SF, Bullock MW. 2008. Low-frequency electrical properties of polycrystalline saline ice and salt hydrates. *J. Phys. Chem. B* **112**: 15382.
- Hauck C. 2013. New concepts in geophysical surveying and data interpretation for permafrost terrain. *Permafrost and Periglacial Processes* **24**, 131-137.
- Hauck C, Bottcher M, Maurer M. 2011. A new model for estimating subsurface ice content based on combined electrical and seismic data sets. *Cryosphere* **5**: 453-468.
- Heginbottom J, Brown J, Humlum O, Sennson H. 2012. Permafrost and periglacial environments, In State of the Earth's Cryosphere at the Beginning of the 21st Century (eds. R. Williams and J. Ferrigno). *USGS Professional Paper* **1386-A-5**, 546 pp.
- Jorgenson MT, Osterkamp TE. 2005. Response of boreal ecosystems to varying modes of permafrost degradation. *Can. J. For. Res.* **35**: 2100-2111.
- Jones D. 1997. Investigation of Clay-Organic Reactions Using Complex Resistivity, MS Thesis, Colorado School of Mines, 378 pp.
- Kanevskiy M. 2008. Detailed cryostratigraphic studies of syngenetic permafrost in the winze of the CRREL permafrost tunnel, Fox, Alaska. *Conf. Permafrost*.
- Kemna A, Binley A, Ramirez A, Daily W. 2000. Complex resistivity tomography for environmental applications. *Chem. Eng. J.* **77**: 11-18.
- Kim JH, Yi MJ, Park G, Kim JG. 2009. 4-D inversion of DC resistivity monitoring data acquired over a dynamically changing earth model. *J. Appl. Geophys.* **68**: 522-532.
- Kneisel C, Hauck C, Fortier R, Moorman B. 2008, Advances in geophysical methods for permafrost investigations. *Permafrost Periglacial Proc.* **19**: 157-178.
- Loke MH, Barker RD. 1996. Rapid least-squares inversion of apparent resistivity pseudo-sections using quasi-Newton method. *Geophys. Prosp.* **48**: 152-181.
- Minsley, BJ, and 12 others. 2012. Airborne electrical imaging of discontinuous permafrost. *Geophys. Res. Lett.* **39**: doi:10.1029/2011GL050079.
- Olhoeft GR. 1977. Electrical properties of a natural clay permafrost. *Can. J. Earth Sci.* **14**: 1977,

16-24.

Olhoeft GR. 1985. Low-frequency electrical properties. *Geophysics* **50**: 2492-2503.

Petrenko V, Whitworth R. 1999. *Physics of Ice*. Oxford, 373 pp.

Schurr EA, and 18 others. 2008. Vulnerability of permafrost carbon to climate change: implications for the global carbon cycle. *BioScience* **58**: 701-714.

Scott WJ, Sellman PV, Hunter JA. 1990. Geophysics in the study of permafrost. In *Geotech. And Environ. Geophys., Vol 1* (ed. S.H. Ward), *Invest. Geophys*: **5**, Soc. Explor. Geophys., Tulsa, pp. 355-384.

Sellman, PV. 1967. Geology of the USA CRREL Permafrost Tunnel, Fairbanks, Alaska, *CRREL TR 199*, 22 pp.

Sellman PV. 1972. Geology and Properties of Materials Exposed in the USA CRREL Permafrost Tunnel, *CRREL SR 177*, 14 pp.

Stillman, DE., Grimm RE, Dec S. 2010. Low-frequency electrical properties of ice-silicate mixtures., *J. Phys. Chem. B* **114**: 6065-6073.

Stillman DE, MacGregor JF, Grimm RE. 2013. The role of acids in electrical conduction in ice. *J. Geophys. Res.* **118**: doi:10.1029/2012JF002603.

8. Figures

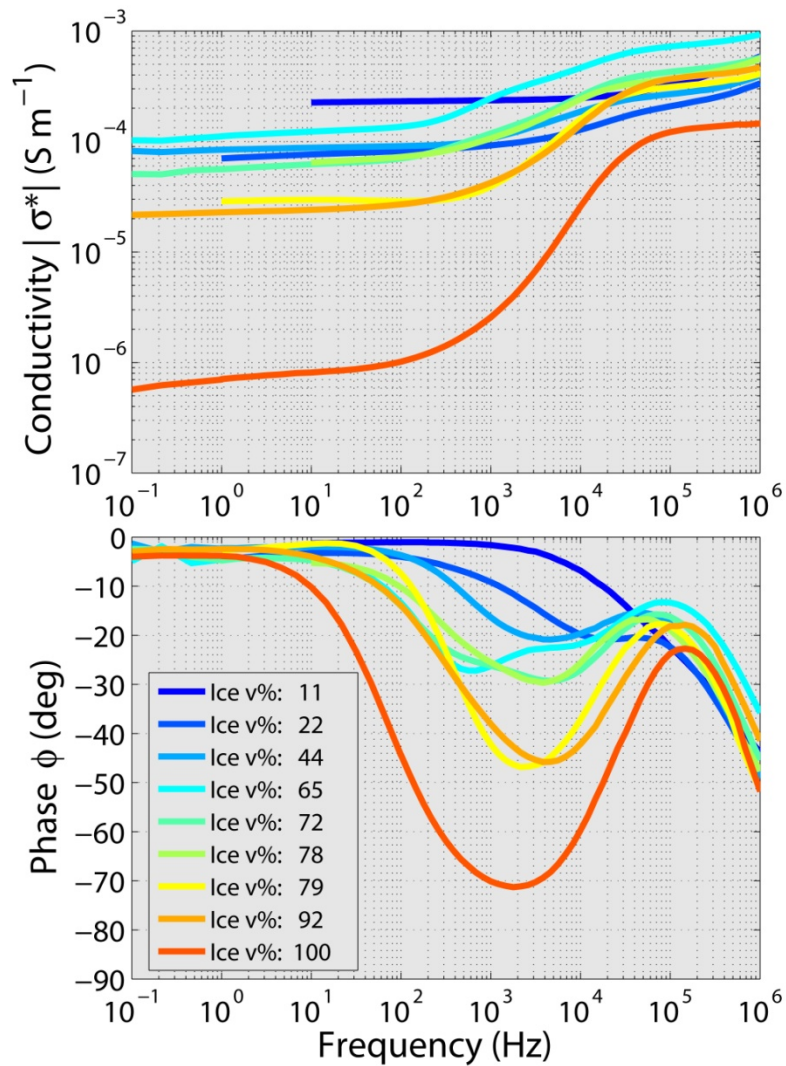


Figure 1. Frequency dependence of the electrical properties of Fairbanks silt as a function of fractional ice volume at fixed temperature of $-3^{\circ}C$. **(a)** Conductivity magnitude. **(b)** Phase. Principal features are DC conduction at low frequency and the dielectric relaxation of ice at high frequency. Samples were acquired in the Fox Permafrost Tunnel and ice content was varied by rehydrating dried samples.

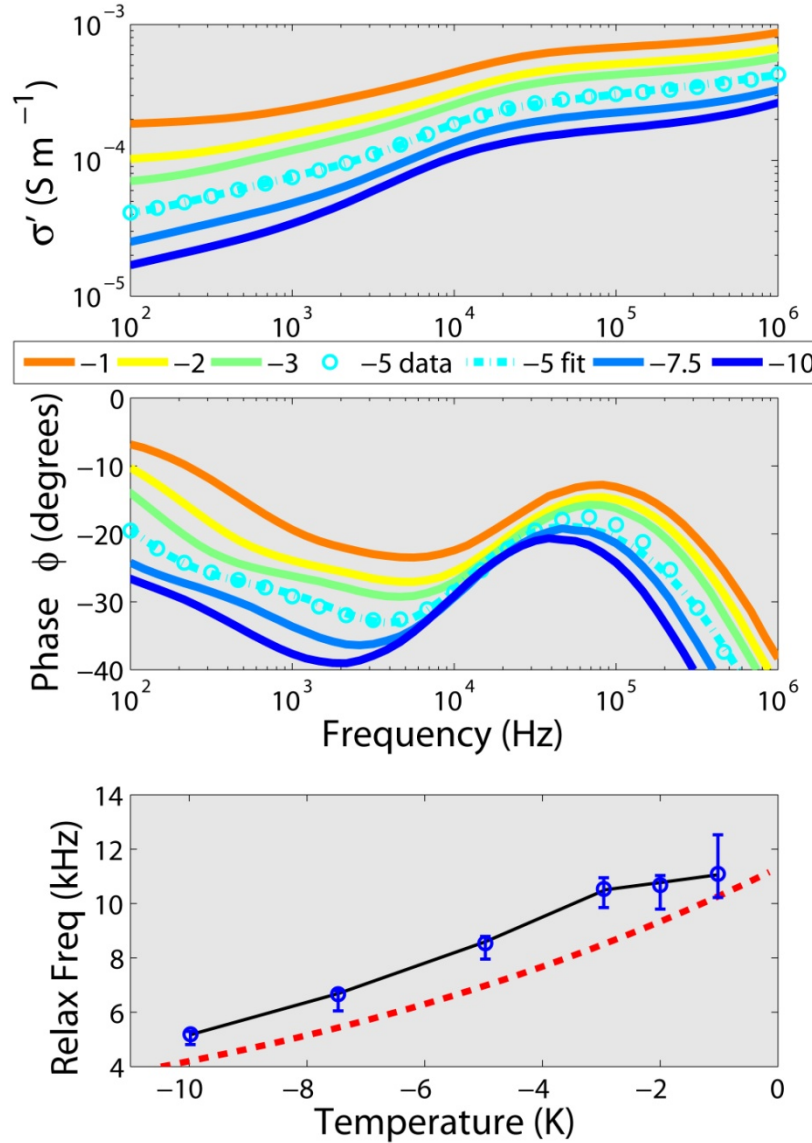


Fig. 2. Frequency dependence of the electrical properties of Fairbanks silt as a function of temperature for fixed ice volume fraction of 72%. **(a)** Real conductivity. **(b)** Phase. **(c)** Relaxation frequency. In practice, several relaxation mechanisms must be fit to each curve in order to accurately extract the ice frequency. Fits were performed between 10 Hz and 20 kHz to simulate field bandwidth. Dashed line shows Auty-Cole relation for “pure” ice; higher frequencies in our samples indicate presence of soluble impurities. Deviation above -3°C is due to premelting in polycrystalline samples. At lower temperatures, relaxation frequency determines temperature to accuracy of $\pm 0.5^\circ\text{C}$.

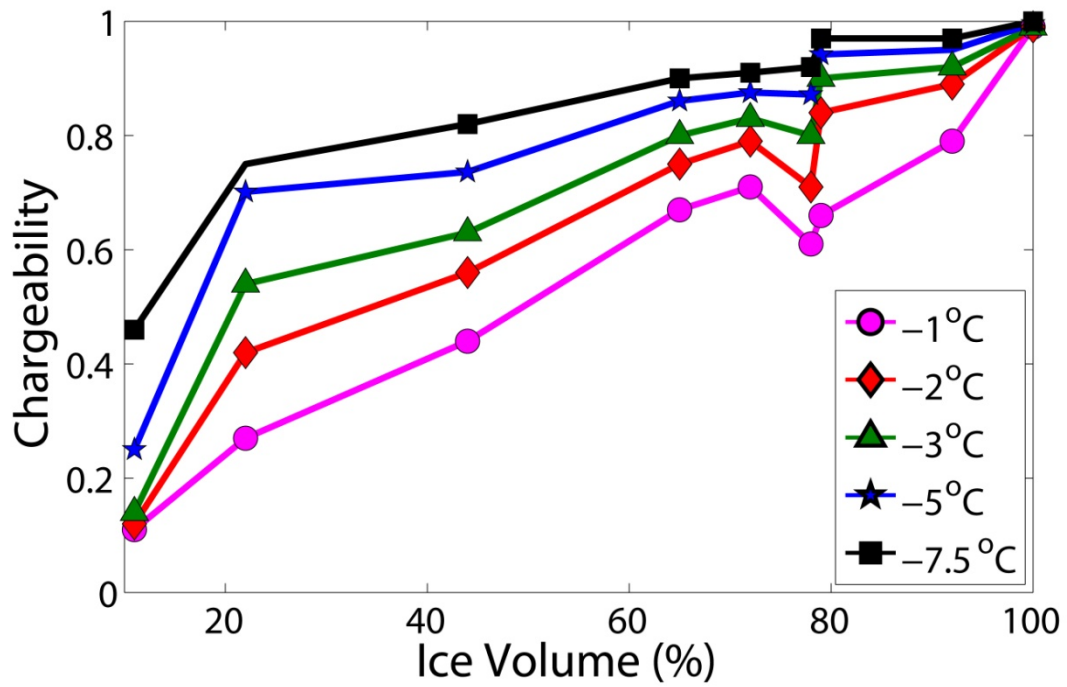


Figure 3. Variation in chargeability $m = (\sigma'_{20\text{kHz}} - \sigma'_{10\text{Hz}}) / \sigma'_{20\text{kHz}}$, where $\sigma'_{10\text{Hz}}$ and $\sigma'_{20\text{kHz}}$ are the real conductivities at 10 Hz and 20 kHz, respectively. Monotonic curve fits are used to invert ice volume from chargeability at each temperature.

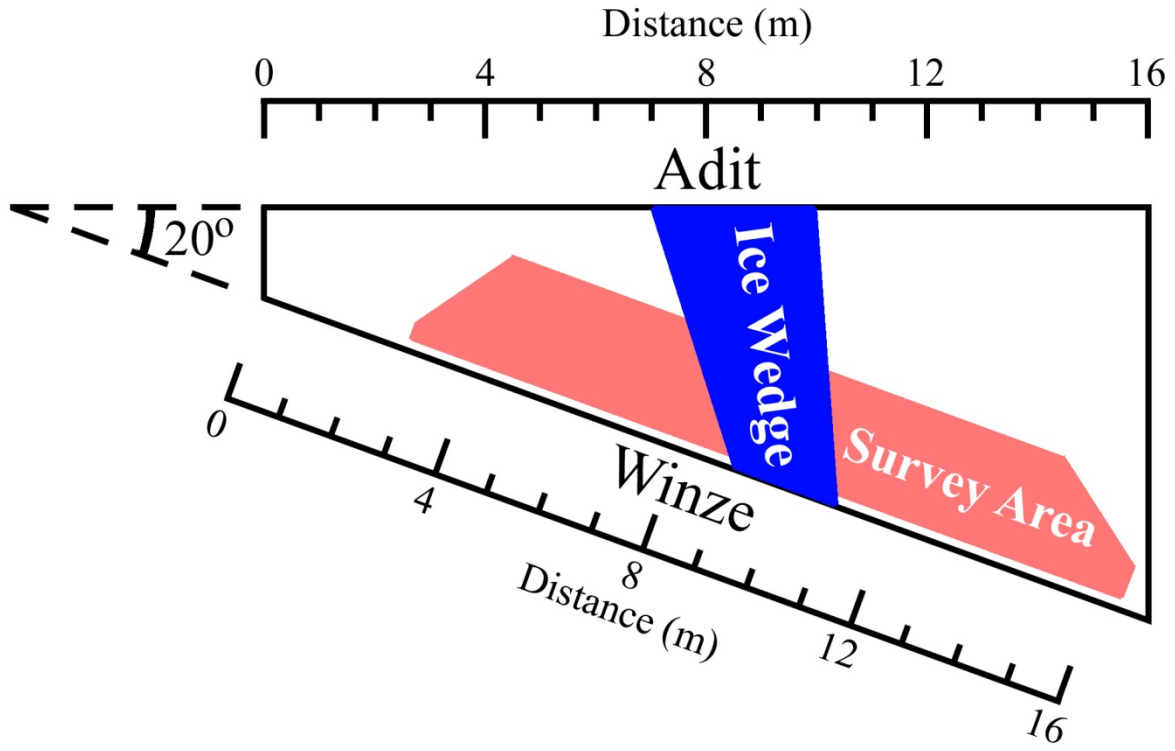


Figure 4. Horizontal projection of adit-winze intersection in the Fox Permafrost Tunnel (Sellman, 1972), with position of ice wedge taken from Arcone (1984). SIP survey performed along the winze wall using 16 electrodes at locations 1–17 m; the interior area imaged is shaded.

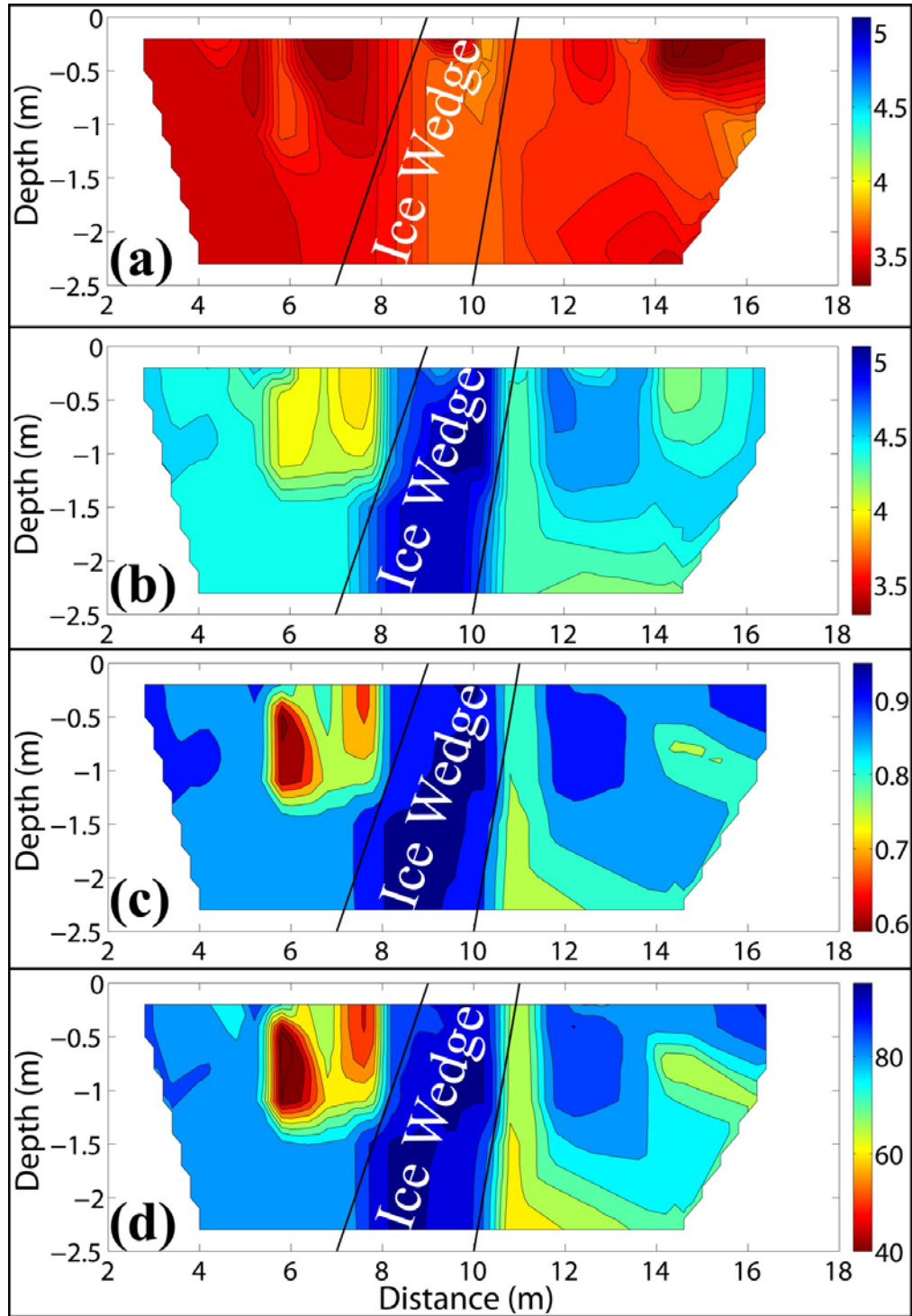


Figure 5. SIP horizontal section (2D survey/interpretation) into the north wall of the Fox Permafrost Tunnel winze. Coordinates and position of ice wedge follow Fig. 4. **(a)** HF (20 kHz) resistivity, **(b)** LF (10 Hz) resistivity, **(c)** chargeability, and **(d)** ice content, derived using laboratory measurements at -3°C (Fig 3).

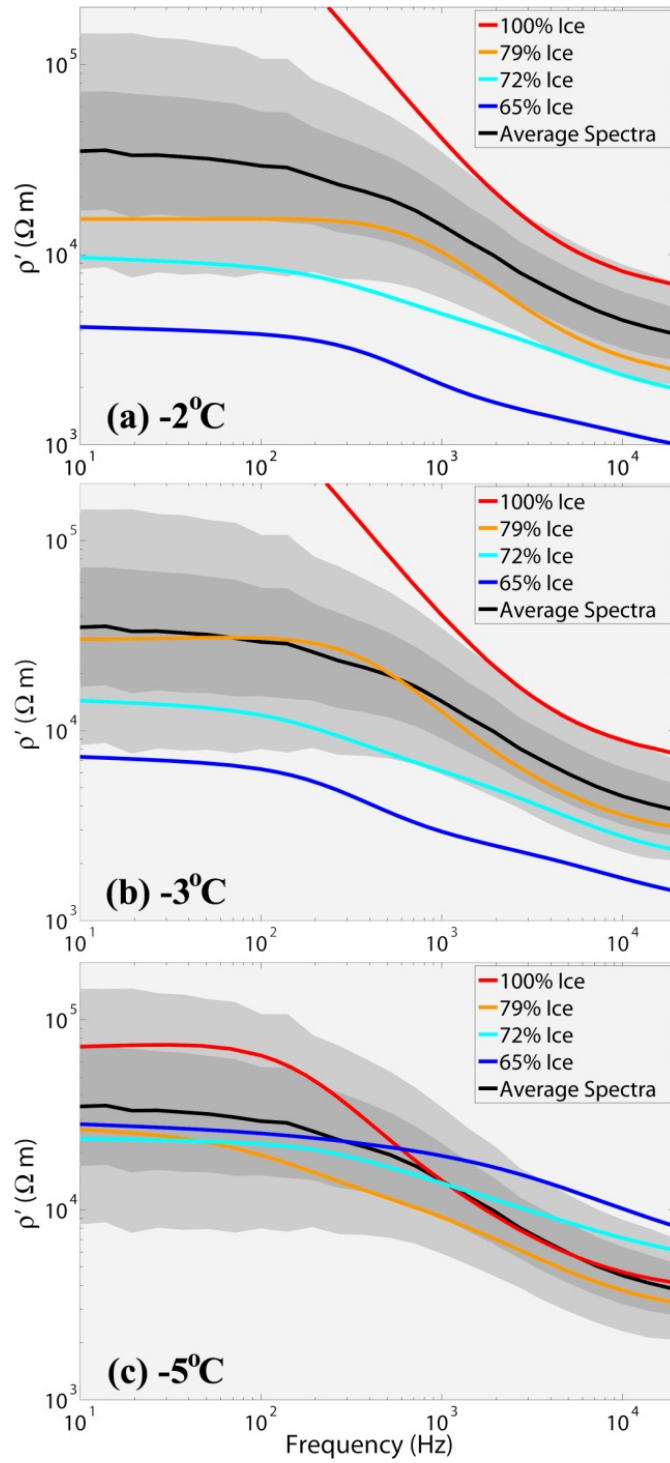


Figure 6. Comparison of laboratory data (color) to ensemble of inverted field data (black = mean, dark gray = 68th percentile, light gray = 95th percentile). Best fit is at -3°C .